JOURNAL OF SPACECRAFT AND ROCKETS
Vol. 32, No. 4, July–August 1995

Metal-Oxide-Silicon Capacitor Detectors for Measuring Micrometeoroid and Space-Debris Flux

P. C. Kassel*
NASA Langley Research Center, Hampton, Virginia 23681
and
J. J. Wortman†
North Carolina State University, Raleigh, North Carolina 27695

Capacitor-type micrometeoroid flux detectors have been fabricated and tested. The detectors were of the metal-oxide-silicon type and were formed using standard silicon technology developed for fabricating microelectronic devices and circuits. The detectors were tested using an electrostatic accelerator and carbonyl iron projectiles ranging in size from 0.3 to 5.0 μm in diameter (1×10^{-13} to 5×10^{-10} g) with velocities from 1 to 20 km/s. The detector operation was found to be reliable if the bias voltage was held above a threshold value that is necessary for a significant capacitor discharge. Variations of the bias voltage above the bias threshold did not appear to affect the detector sensitivity. An empirical relationship has been developed relating the sensitivity of the detectors to the detector thickness (dielectric plus top electrode) and the projectile diameter, velocity, and angle of impact. The mechanism responsible for the capacitor discharge appears to be the creation of charge carriers, followed by cascade ionization in the dielectric, caused by an impacting projectile. Once triggered, the discharge is then powered by the charge stored in the capacitor, which forms a plasma (spark) that causes a portion of the top metal electrode to vaporize, creating an open circuit at the impact site (i.e., the discharge self-extinguishes), which then allows the capacitor to recharge. The detector area lost as a result of impact damage is dependent on the discharge energy and is negligible for most applications.

Nomenclature

a	= acceleration voltage, V
C	= capacitance, F
$\cos\beta$	= cosine of impact angle
Dia	= projectile diameter, μm
d	= projectile diameter, m
E	= energy of capacitor discharge, J
KE	= kinetic energy of projectile, J
K_1	= preliminary detector sensitivity parameter, $g^{1/3} \cdot$ (km/s)
K_2, K_3	= preliminary detector sensitivity parameters, $\mu m \cdot$ (km/s)
Mass	= projectile mass, g
m	= projectile mass, kg
p	= projectile momentum, kg · (m/s)
q	= charge on projectile, C
S	= detector sensitivity parameter, $\mu m \cdot$ (km/s) $\cdot \mu m^{-0.875}$
Thck	= detector thickness, μm
Vel	= projectile velocity, km/s
V_b	= detector bias voltage, V
V_s	= detector signal voltage, V
v	= projectile velocity, m/s
β	= angle between velocity and detector normal, deg
ρ	= projectile density, kg/m^3
τ	= time interval, s

Introduction

METEOROID and man-made debris are significant hazards of the space environment. To assess these hazards, several spacecraft missions have had as their primary or secondary objectives the measurement of meteoroids and debris in near-Earth space. In spite of the many successes, the meteoroid and debris environment is still not well known, especially with respect to the low-mass particles generally referred to as cosmic dust or micrometeoroids.

The most basic and probably the most important measurement made concerning dust particles in space is a determination of the flux (the number of particles encountered per unit time per unit area by a spacecraft in a particular orbit). Ideally, particle flux would be measured as a function of the mass, density, velocity, or other characteristics of the particles. Usually this is not possible and compromises must be made. The flux can sometimes be measured as a function of the type of damage or hazard associated with the particles counted. A pressurized cell, for example, has been used to measure fluxes of larger particles, which cause punctures.[1] However, puncture is not the only meteoroid or debris hazard. Particles that cannot significantly damage the spacecraft can damage critical surfaces. If such particles are encountered in large numbers, they will limit the useful life of optical surfaces, windows, thermal coatings, or other spacecraft components that depend on fixed surface properties. The capacitor-type detector has been developed to make time-resolved flux measurements of small meteoroid and debris environments in space, and several hundred of these detectors have flown on the Meteoroid Technology Satellite (MTS, Explorer-46) and the Long Duration Exposure Facility (LDEF) satellite.

The capacitor-type detector[2] is a fairly simple device consisting of a parallel-plate capacitor with a very thin dielectric. The top metal plate (electrode) is made very thin and is the surface that is exposed to the impacting particles. The device is operated with an electrical potential (bias voltage) applied across the capacitor plates; hence a charge is normally stored in the capacitor. When a particle impacts the exposed thin plate with enough energy, it can cause the dielectric to breakdown and result in an internal discharge of the capacitor. The event can be measured by monitoring the charge required to recharge the capacitor. The mechanism responsible for the discharge is complex and will be discussed further in a later section. The sensitivity of the detector depends on a number of factors such as the dielectric thickness, the top-electrode material and thickness, and the applied bias voltage, as well as the physical properties of the impacting particle.

Received Feb. 4, 1994; revision received May 16, 1994; accepted for publication Sept. 28, 1994.

*Aerospace Technologist, Acoustic, Optical, and Chemical Measurement Branch, Experimental Testing Technology Division.

†Professor, Electrical and Computer Engineering Department.

Some calibration work on detectors of this type[3] has been done using the Goddard Space Flight Center accelerator (a two-million-volt accelerator), which is similar to the Langley Research Center accelerator described later and used for the present work. In that work the researchers investigated metal-dielectric-silicon detectors using silicon dioxide and silicon nitride as the dielectric with thicknesses ranging from 0.4 to 4.0 μm. They also investigated both Al and Au metal electrodes with thicknesses ranging from 0.05 to 0.2 μm. The results of their tests were very encouraging. However, the number of tests they were able to perform was limited and indicated the need for a more extensive study to determine the level of calibration needed for this type of detectors.

The purpose of the present work has been to repeat and expand on the experiments previously reported[4] on the metal-oxide-silicon (MOS) capacitor detectors with the aim of developing a more accurate calibration of the detectors. Based on our results coupled with the previous work, it has been possible to design and carry out a very successful experiment (Interplanetary Dust Experiment, or IDE) on LDEF.[5]

Detector Fabrication

The technology used to fabricate the detectors is based on the silicon technology widely used in the manufacture of microelectronic devices and circuits. Figure 1 shows a cross section and Fig. 2 is a photograph of a sensor. The substrate (bottom electrode) of the detectors used in these studies consisted of silicon wafers, 2 in. in diameter, and polished on one side (top side or sensitive surface) by a combination of mechanical polishing and electropolishing. The silicon wafers were p-type with resistivities of less than 0.01 $\Omega \cdot$ cm. The fabrication process consists of the following steps: 1) substrate cleaning, 2) thermal oxidation of the silicon wafer to form the capacitor dielectric, 3) removal of a portion of the oxide on the unpolished (back) side of the wafer to gain access to the silicon to form an electrical contact, and 4) evaporation of aluminum on both faces of the wafer to form the top capacitor electrode and electrical contact to the silicon wafer. Wafer cleaning consisted of a typical RCA cleaning followed by a rinse in de-ionized water and drying using dry nitrogen. The thermal oxide was grown in a standard oxidation furnace using a quartz tube. A dry-wet-dry oxidation process was used in which the wafer was first exposed to dry oxygen for 5 min, followed by a wet cycle for the appropriate time (the time being chosen to give the desired oxide thickness), which was then followed by an additional 5-min dry cycle. The wet process was used to reduce the oxidation time below that which would have been required if dry oxygen were used for the total oxidation cycle. Typically, the oxides were grown at 1100°C.

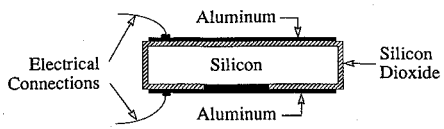

Fig. 1 Cross-sectional view of a metal-oxide-semiconductor detector.

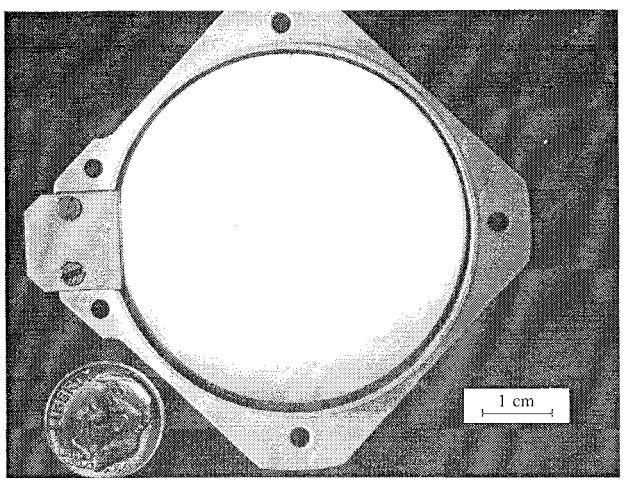

Fig. 2 Micrometeoroid impact detector.

Following the oxidation, a hole was etched in the oxide on the back side of the silicon wafers by first placing them on a flat surface with the unpolished side facing up. A crystallite of ammonium bifluoride was then placed at the center of the wafer. A drop of water was then placed on the ammonium bifluoride crystal which formed hydrogen fluoride ions which etched the oxide. The area removed depended on the size of the crystal and the amount of water added. The typical etch area was approximately 1 cm in diameter. Following the etch, which took approximately 5 min, the wafer was thoroughly rinsed in de-ionized water. The wafers were then dipped in acetone and then in hot Transene™. This was followed by drying with dry nitrogen. The wafers were then loaded into a vacuum evaporator where the backside metal was evaporated on to the wafers. This step was followed by turning the wafers over and evaporating metal on the front side. A shadow mask was used to define the metal, and an unmetallized edge was left on the wafers, which was approximately 0.075 cm wide. Following metallization the wafers were annealed in dry nitrogen at 200°C to sinter the metal. A variety of dielectric thicknesses were investigated, ranging from 0.4 to 1.7 μm. Aluminum with a nominal thickness of 0.1 μm was used for the top and bottom metal.

After fabrication the detectors were tested electrically by connecting them to a curve tracer to measure the internal leakage of the capacitor. Typically the capacitors were found to be shorted at this stage. However, the shorts could be removed by connecting a resistor (5–100 kΩ) in series with the capacitor and turning up the voltage on the curve tracer. As the voltage is increased, Joule heating, caused by high currents in the defects regions, burns (evaporates) away the thin top-electrode metal in the vicinity of the defect, and hence the defect region is removed from the electrical circuit of the capacitor. Also, as the voltage is increased to higher values, weak spots in the capacitor tend to break down, again burning away the metal electrode at the point of breakdown. The maximum voltage that the capacitor can withstand depends on the dielectric strength of the silicon oxide, which is approximately 10 MV/cm. When breakdown occurs it is usually accompanied by a flash of light that can easily be seen with the naked eye. The voltage used to clear a capacitor detector was chosen according to the thickness of the dielectric.

Impact Facilities and Test Instrumentation

Micrometeoroid impact simulators located at Langley Research Center and Goddard Research Center were used to perform the impact tests on the detectors (those facilities are now closed). The two facilities produced similar particles; hence only the Langley facility[6] will be described here. A 4-MV Van de Graaff generator was used to accelerate charged carbonyl iron projectiles 0.3 to 5 μm in diameter (1×10^{-13} to 5×10^{-10} g) to velocities from 1 to 20 km/s. These facilities were particularly well suited for these tests in that the mass of the projectiles was in the range of the expected sensitivity of the detectors. Another significant feature of these facilities was the absence of gun debris and acceleration gases that occur in light-gas gun and plasma accelerators.

The major advantage of the electrostatic accelerator was that the projectiles were charged and therefore easy to measure and control. After being accelerated by the Van de Graaff accelerator, the projectiles entered the instrumented control section of the beam line. In this section of the simulator, a computer controlled the projectile and recorded the measurements made on the particle. The time of flight for each projectile was measured over a 1-m flight path. If this time was within a preselected range, an electronic gate was opened to allow only that projectile to proceed to the target. For each projectile selected, out of the many accelerated, three measurements were recorded: 1) the charge q on the projectile, 2) the time of flight τ over the 1-m flight path, and 3) the accelerator voltage a. From these three measurements, projectile parameters such as the kinetic energy KE, velocity v, mass m, and momentum p were calculated.

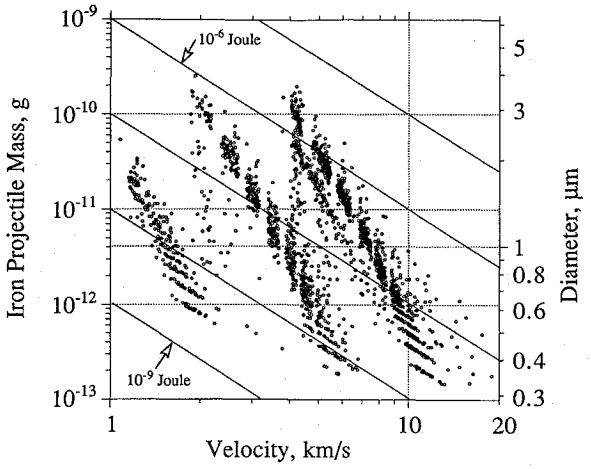

Fig. 3 Projectile mass, diameter, and kinetic energy vs velocity for various accelerator voltages.

The projectile diameter d was also calculated assuming a spherical shape and uniform density ($\rho = 7860$ kg/m^3) of the projectile:

$$\mathrm{KE} = mv^2/2 = qa \tag{1}$$

$$v = 1.000/\tau \tag{2}$$

$$m = 2qa\tau^2 \tag{3}$$

$$p = 2qa\tau \tag{4}$$

$$d = (12qa\tau^2/\pi\rho)^{\frac{1}{3}} \tag{5}$$

There were some inconveniences associated with the electrostatic accelerator, however. The projectile mass and velocity could not be selected or controlled independently, because the accelerator produced a sequence of projectiles that conformed, more or less, to the relationship $dv^2 =$ constant. This was expected, since the projectiles were likely to be charged to a uniform surface charge density. To alleviate this problem, the accelerator was operated at three different voltages (4, 1, and 0.5 MV). Figure 3 is a plot of the projectile parameters for all the tests included in this report. This figure illuminates some of the problems with this data set. For example, the clustering of projectiles along lines of constant energy was due to the resolution in the measurement of the accelerator voltage (10 kV) and the projectile charge (1.5×10^{-15}C). These measurements were the largest source of error in the determination of the projectile mass or diameter, and in subsequent plots error bars are shown when this error exceeds 10% of the mass. Clustering of projectiles in velocity regions was the result of the accelerator control system rejecting projectiles near the edge of the velocity selection windows.

The projectiles were focused so that they impacted in an area approximately 1 to 3 mm in diameter. The position of the detector was controlled vertically and horizontally with a precision of approximately 1 mm. The angle of impact was varied from 0 to 75 deg from the normal to the target with an error of approximately 1 deg. For normal impacts, it was possible to have a well-defined target area 5–7 mm in diameter. Most tests were at room temperature; however, for thermal environmental impact tests, a target chamber with heating elements and a liquid-nitrogen coil was used to obtain impacts on sensors at +95 and −100°C.

A schematic diagram of the instrumentation used to measure the detector signals is shown in Fig. 4 along with a sketch of a typical signal. The signal parameters of interest were the time of occurrence, the rise time, and the amplitude. The recovery time was fixed by the time constant RC of the detector circuit, where R is the bias resistance (1 MΩ) and C is the detector capacitance. Recovery itself is more important than recovery time, and a qualitative determination of the detector recovery was made by comparing the detector leakage current after a test with its value before the test. If the leakage current was unchanged, the detector was assumed to have recovered.

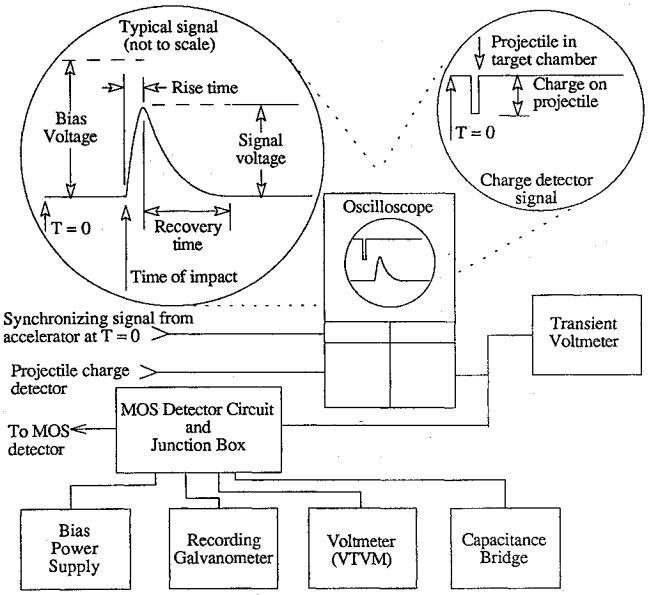

Fig. 4 Block diagram of instrumentation used for MOS detector calibration test.

A dual-beam oscilloscope (Fig. 4) was the primary means of measuring the signal parameters and correlating the signal with the impacting particle. The oscilloscope was triggered by the accelerator when a particle was selected for entry into the target chamber. For the calibration tests that are reported here, the instrumentation (similar to that used in the characterizing test of Ref. 4) included an in-flight projectile detector located at the entrance to the target chamber. This detector was similar to those used in the accelerator beam control section, and its output was monitored with one beam of the oscilloscope to provide an independent measure of the projectile charge and velocity. This detector provided a reliable way of knowing, in the absence of any signal from the MOS detector, that a particle impact (a "no signal" event) did occur. The second beam of the oscilloscope was used to look for low-level signals (from the MOS detector) at the expected time of impact, and the transient voltmeter measured the voltage level of discharge signals that exceeded the range of the oscilloscope. Also, a galvanometer with a slow-moving strip-chart recorder was used to continuously monitor the current to the MOS detector. This galvanometer had a high current sensitivity but poor response time; however, it could detect discharge signals and would have indicated any signals that were not synchronized with the impacting particle.

Impact Tests

The impact tests described here are divided into two overlapping categories. First are the tests that define or characterize the operation of the MOS detector. Because the function of the detector is to convert an impact event into an electrical signal that can be counted and correlated to the time of impact, these tests were concerned with the time and magnitude of the signal versus the detector bias voltage and thickness. For this category of tests, the parameters of the impacting particle are significant only to the extent that the impact event was above the detector's threshold of sensitivity. The end result of these tests was to define a minimum level of bias voltage (bias threshold), above which the detector was considered to be reliable and consistent when counting impact events. Also included in this category are tests that demonstrate the detector operation over a wide temperature range.

The second category of tests consists of those that provide a calibration of the MOS detectors by defining the detector's threshold of sensitivity. In these tests the detector bias voltage was always above the bias threshold (determined above) and the parameters of the impact event varied so that the detector would either 1) produce a signal, indicating the impact was above the sensitivity threshold, or 2) give no response, indicating the impact was below the sensitivity threshold.

Characterization Tests

The signals measured using the test arrangement described earlier are classified according to amplitude into two types—those greater than 1 V (called discharge signals) and those less than 1 V (called low-level signals). Although this classification may seem arbitrary, the difference between the two types of signals is substantial, as can be seen in Fig. 5, where signal amplitude is plotted as a function of applied voltage for four detector thicknesses from 0.5 to 1.8 μm (dielectric thicknesses of 0.4, 0.7, 1.0, and 1.7 μm). The discharge time (rise time of both types of signal) was approximately 0.5 μs for the 1.1-μm detectors and 1.5 μs for the 0.5-μm detectors. As might be expected, the greater the bias voltage, the fewer the low-level signals. Above some bias threshold there are few, if any, low-level signals, indicating that the detector will essentially respond as an event counter, assuming that the impacting projectile has enough energy to cause any response at all from the detector. Figure 6 is a plot similar to that of Fig. 5 except that a linear scale is used and all signals for a given bias voltage are averaged. As indicated in Fig. 6, the average signal appears to be dependent only on the bias voltage and is significantly influenced by its polarity. As can be seen in Figs. 5 and 6, a bias voltage greater than approximately 35 V on any of these detectors is enough to exceed the required bias threshold. One would expect the bias threshold voltage to scale with the electric field; however, this does not appear to be the case. Although there is a slight dependence on the thickness, it is far from what a direct field dependence would require. The relationship between the bias threshold voltage and the projectile parameters will be discussed later.

Recovery of the detector after an impact was usually very good, with the leakage current less than 1 nA. Occasionally a low-level signal was followed by a temporarily increased or erratic leakage current (10–100 nA). In one test, a detector was completely discharged and did not recover when it was inadvertently subjected to a stream of particles (approximately 60 per second) for a few seconds. The problem here is that there is not enough current flowing

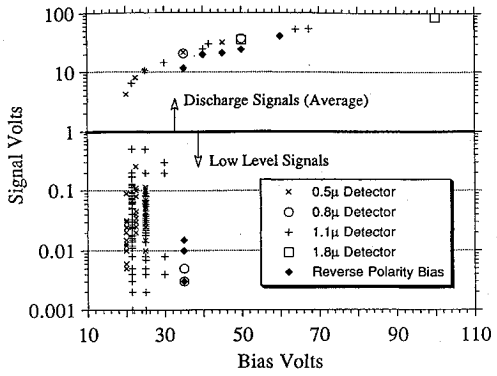

Fig. 5 Signal amplitude vs detector bias voltage for various detector thicknesses.

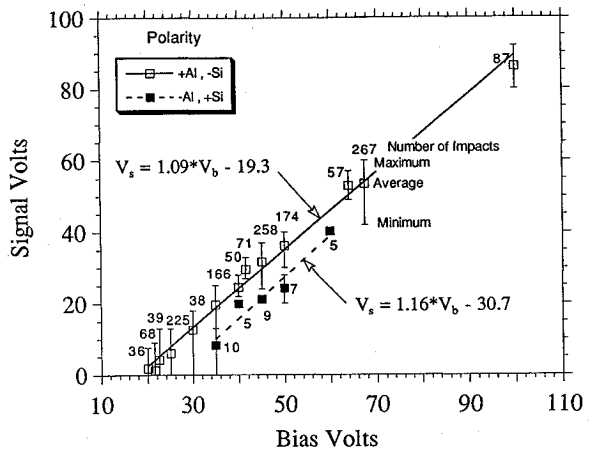

Fig. 6 Average signal voltage vs bias voltage for detector thicknesses of 0.5, 0.8, 1.1, and 1.8 μm.

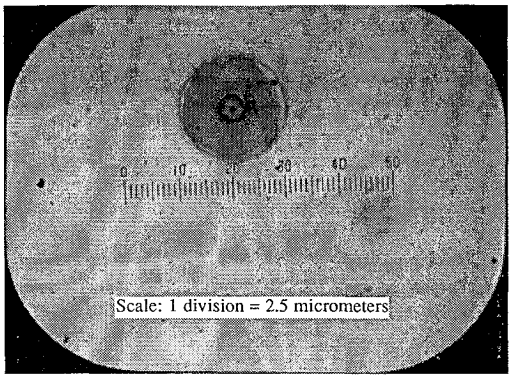

Fig. 7 Photomicrograph of impact signal crater on a 1.1-μm detector with 60-V bias.

in any given damaged region of the detector to burn away the top electrode material. This will be discussed later.

The impacted areas were visually inspected following impact tests to determine the characteristics of the events. For the case of low-level signals, the impact damage is confined to an area just slightly larger than the crater caused by the impacting projectile. In sharp contrast, the impacts that caused a discharge signal resulted in a damaged area ranging from 10 to 100 μm in diameter, depending on the test conditions, and in particular the bias voltage. Figure 7 is a photomicrograph of a typical impact site which resulted in a discharge signal. As can be seen, the damaged area is nearly circular. Upon close examination one finds that the top-electrode material is vaporized away throughout the total damaged areas. However, the dielectric remained intact except for the central part (~10 μm) of the impact feature. In this central region where the impact occurred, the dielectric layer has been removed and the underlying silicon exposed. The nature and extent of the damaged region is far greater than that caused by the projectile alone, as will be discussed later in the paper.

Tests were conducted to determine if a relationship exists between the type of signal and the projectile parameters. These data are plotted in Figs. 8–11. In these figures each data point represents an impacting projectile according to its velocity and diameter. The type of symbol used in the figures represents whether a discharge occurred, a low-level signal was recorded, or no signal was recorded. These tests repeat and extend the analysis of similar tests reported in Ref. 4, but with much greater confidence in the no-signal events because of the added in-flight projectile monitoring. Based on the earlier preliminary calibration of Ref. 4, all of these tests were expected to produce some response from the detector. As can be seen from the data plotted in Figs. 8–11, there does not appear to be any correlation between the signal type and the projectile parameters that might indicate a threshold of projectile sensitivity.

What is very important is the fact that a minimum or threshold of bias voltage is required before the detector will respond to impacting particles in a consistent manner. This can clearly be seen by comparing the data in Fig. 8 with those in Fig. 9, where the detector bias was increased from 20 to 25 V. As seen, the number of no-signal events is drastically reduced, from 32% to 4% of total impacts, with an increase of only 5 V. Similarly, comparing the data of Fig. 10 with Fig. 11 (thicker dielectric and lower electric field strength) shows a decrease in the number of low-level signals (63% to 14%) for an increase in bias voltage of only 5 V.

There is a relationship between the discharge signal and the damaged area, as can be seen in Fig. 12. The detector signal energy E can be calculated and is the difference between the energy stored in the detector (capacitor) before impact and the energy remaining after impact:

$$E = \tfrac{1}{2}CV_b^2 - \tfrac{1}{2}C(V_b - V_s)^2 \qquad (6)$$

where C is the capacitance of the detector, V_b is the magnitude of the bias voltage, and V_s is the signal voltage. This energy range is approximately 10 to 200 μJ. By comparison, the kinetic energy of the projectiles (for these data) was 0.2 to 6 μJ, and their diameter

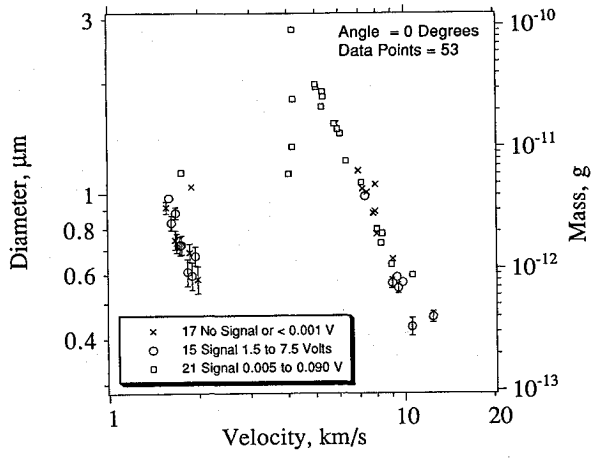

Fig. 8 Projectile parameters vs type of signal for 0.5-μm detector at 20-V bias.

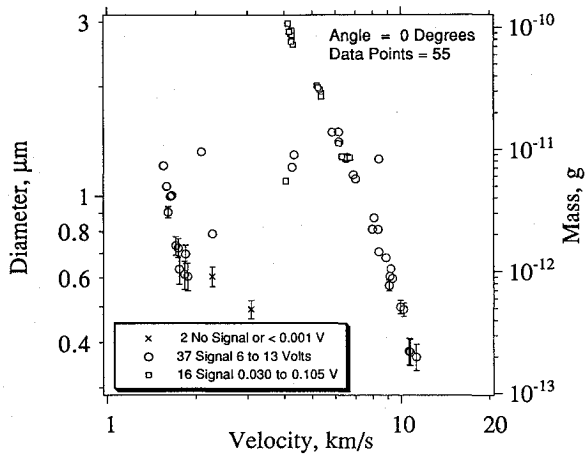

Fig. 9 Projectile parameters vs type of signal for 0.5-μm detector at 25-V bias.

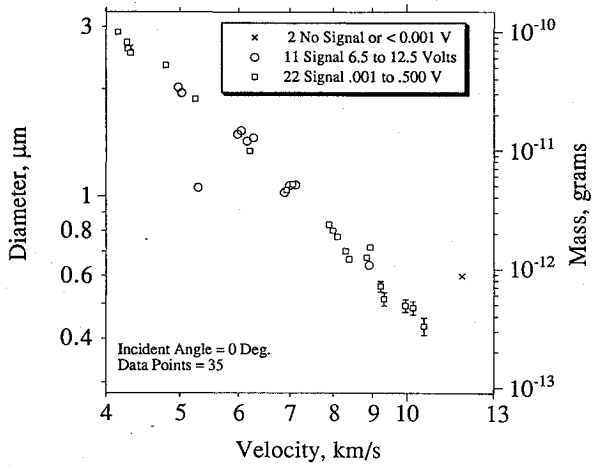

Fig. 10 Projectile parameters vs type of signal for 1.1-μm detector at 25-V bias.

range was 0.4 to 4 μm. This clearly shows that the energy stored in the capacitor plays an important role in the discharge mechanism and crater formation.

Another series of tests investigated the effects of operating at various temperatures that these detectors may be subjected to in the space environment. The results of these experiments are shown in Fig. 13. As can be seen, the detectors operate over the temperature range −100 to +95°C. However, there was a definite decrease in signal voltage for a given bias voltage at lower temperatures.

The effects of operating with a positive bias voltage on the bottom (Si) electrode were studied. As can be seen from the data plotted in

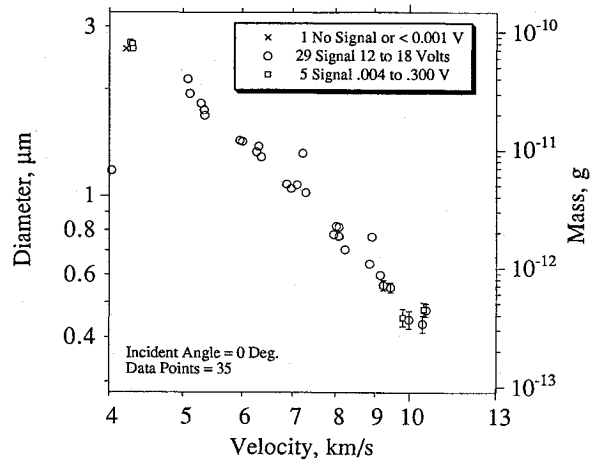

Fig. 11 Projectile parameters vs type of signal for 1.1-μm detector at 30-V bias.

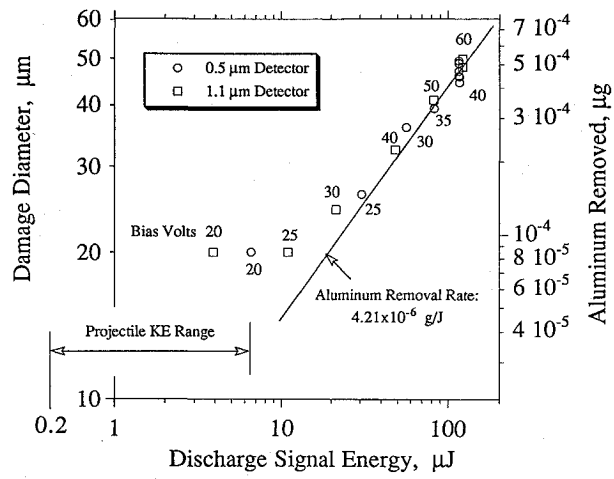

Fig. 12 Diameter of damage area vs discharge signal energy.

Figs. 5, 6, and 13, the signal voltage is significantly reduced if the polarity of the detector bias voltage is switched from a negative bias on the Si substrate to a positive bias. Also, in Ref. 4, the shape of the discharge region for the positive Si bias was not the usual round shape that was found for the negative bias. Although the discharge energy was less, the area affected was greater and irregular in shape.

Calibration Test

Extensive tests (>4000) were run to determine the sensitivity of the detectors to projectile mass, velocity, and impact angle for different detector biases and dielectric thicknesses. In these calibration tests, either a discharge or a low-level signal was regarded as a detector response, and the minimum detectable voltage level for a response was about 1 mV. Four dielectric thicknesses were used for these tests: 0.4, 0.7, 1.0, and 1.7 μm; and the top electrode was 0.1 μm of aluminium for all detectors. Figures 14–17 are typical plots of mass versus velocity for fixed dielectric thickness, bias voltage, and impact angle. As can be seen from the plotted data, there are mass and velocity values that clearly cause discharges; values that did not result in discharges; and values at which discharges are sometimes seen and sometimes not. This overlap region probably occurs because the dielectric breakdown process is complex and statistical in nature, depending on many other factors such as variations in the particle geometry (i.e., not perfect spheres as assumed), variations in the dielectric, and variations in the top-electrode thicknesses. In the use of these detectors, it will be necessary to tolerate some statistical error and uncertainty in the sensitivity near the lower end of the detectivity curve.

Since no satisfactory theoretical model is available for the sensitivity, we have attempted to develop an empirical model through curve fitting of the experimental data. To do this, we first made

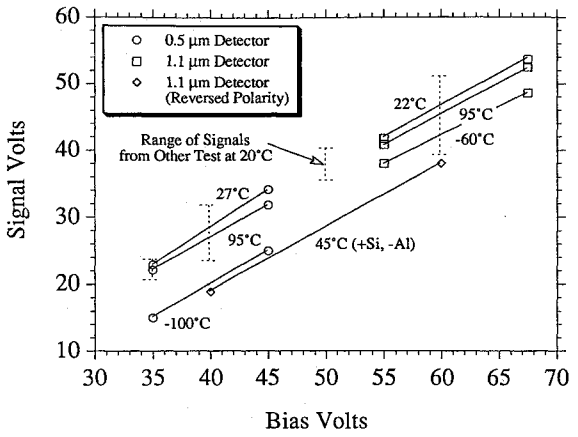

Fig. 13 Signal vs bias voltage at various temperatures.

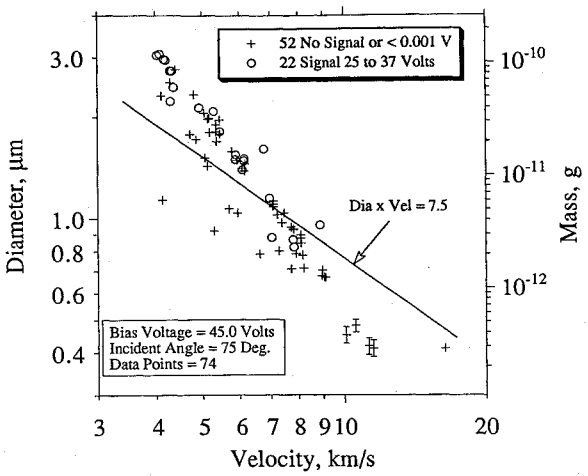

Fig. 14 Typical calibration test results for 0.5-μm detector.

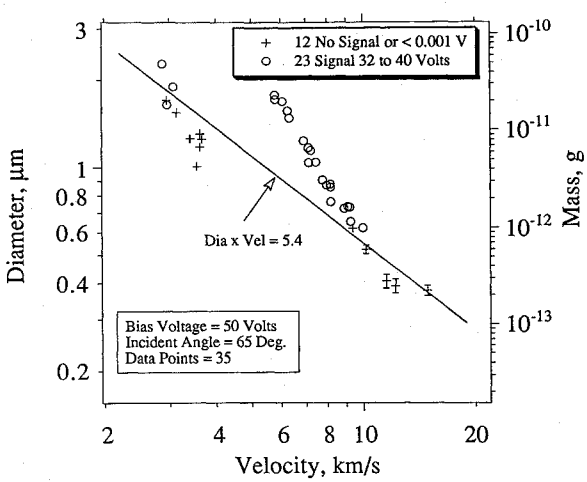

Fig. 15 Typical calibration test results for 0.8-μm detector.

logarithmic plots of mass versus velocity for each angle of impact, dielectric thickness, and bias voltage, as shown, for example, in Figs. 14–17. From these plots it was found that the data could be reasonably fitted to a power series of the form

$$(\text{Mass})^{0.33}(\text{Vel}) = K_1 = \text{constant} \tag{7}$$

or

$$(\text{Dia})(\text{Vel}) = K_2 = \text{constant} \tag{8}$$

Once this relationship was established, we plotted the product of diameter and velocity as a function of the cosine of the impact angle ($\cos\beta$), as measured from the normal to the target, for a given

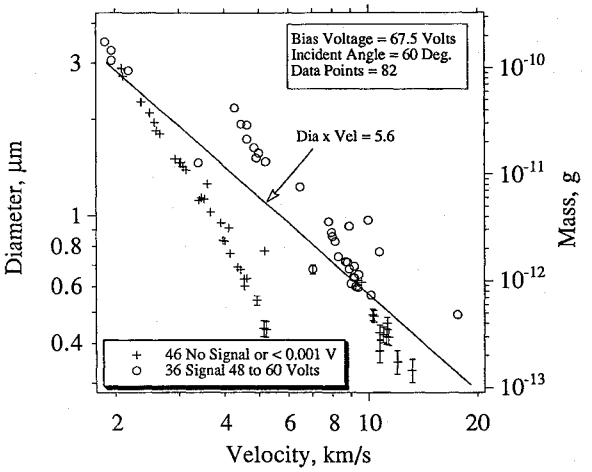

Fig. 16 Typical calibration test results for 1.1-μm detector.

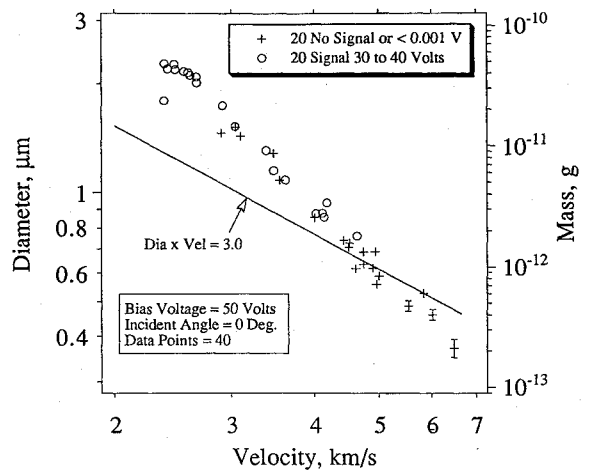

Fig. 17 Typical calibration test results for 1.8-μm detector.

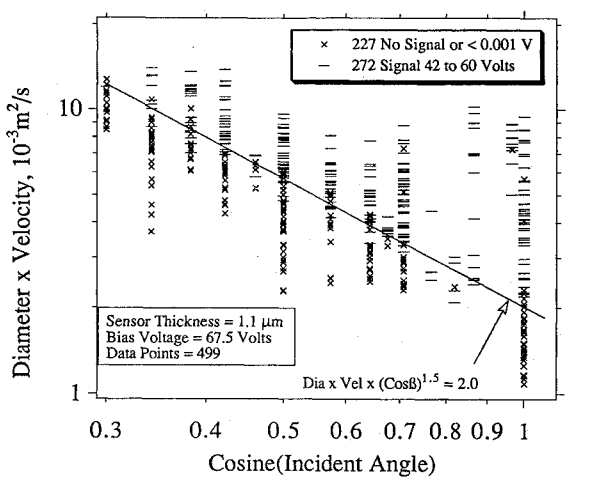

Fig. 18 Typical calibration data as a function of the angle of impact as measured from the sensor normal.

dielectric thickness and bias voltage. Figure 18 is an example of such a plot. From these data we established the following:

$$(\text{Dia})\ (\text{Vel})\ (\cos\beta)^{1.5} = K_3 = \text{constant} \tag{9}$$

Using this relationship, we computed K_3 as an impact calibration parameter and examined this parameter as a function of the applied bias voltage and sensor thickness. Since a large number of points are plotted, a stacked histogram is used to display these relationships, and although the range of the impact parameter is from 0.5 to 15, only the data near the sensitivity threshold are plotted. Figures 19–22 are the primary calibration data (data at lower bias voltage can be

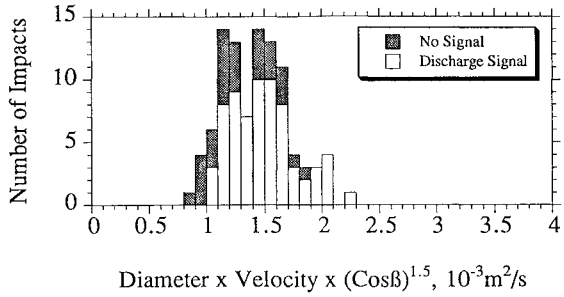

a) Impacts at 35-V bias

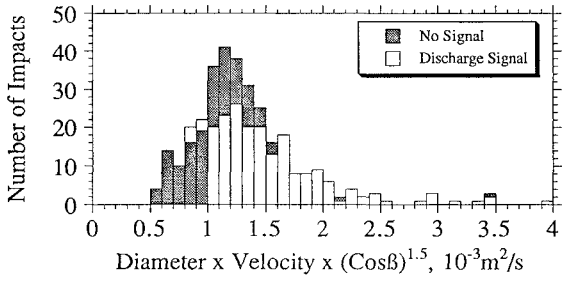

b) Impacts at 45-V bias

Fig. 19 Calibration data for 0.5-μm sensor.

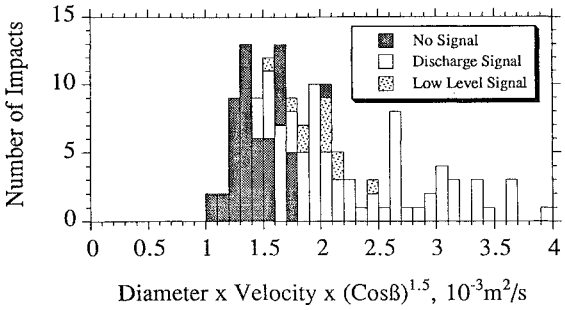

a) Impacts at 35-V bias

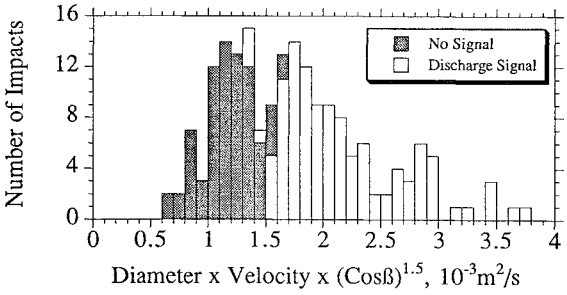

b) Impacts at 50-V bias

Fig. 20 Calibration data for 0.8-μm sensor.

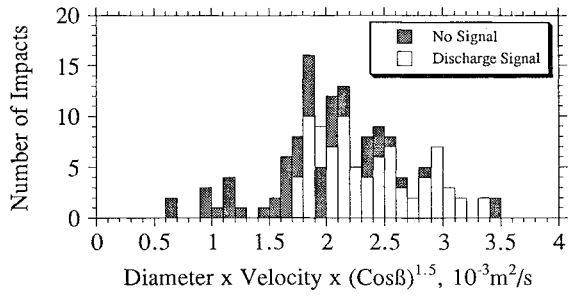

a) Impacts at 40–41.5-V bias

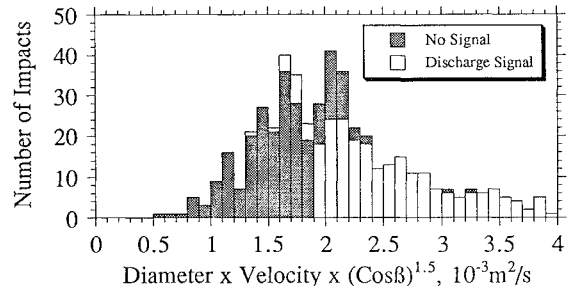

b) Impacts at 64–67.5-V bias

Fig. 21 Calibration data for 1.1-μm sensor.

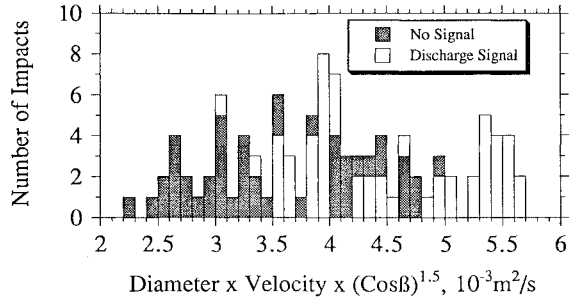

a) Impacts at 50-V bias

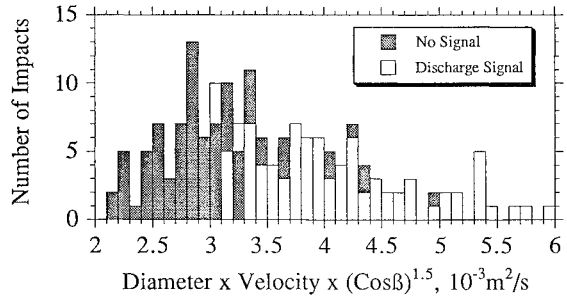

b) Impacts at 100-V bias

Fig. 22 Calibration data for 1.8-μm sensor.

compared, but not used for calibration). As can be seen in these figures, there is little dependence of the sensitivity on the applied bias voltage if the voltage is above the threshold, as discussed earlier. The unexpected low-level signals in Fig. 20 occurred at incident angles of 50 deg or greater and are a good example of the effects of bias voltage for impacts near the sensitivity threshold.

From these figures, one can determine a value for the calibration parameter K_3 for each sensor thickness (dielectric plus top metal) directly from the data at the higher bias voltage. For example, the data for the 0.8-μm sensor in Fig. 20 indicate that for values of K_3 less than 1.5 there will most likely be no response from the sensor and for values greater than 1.5 the sensor will most likely respond with a high-level signal. For the 1.8-μm sensor (Fig. 22), the statistics are improved by combining the data for both bias voltages to obtain a value of 3.3 for K_3.

By plotting these values of K_3 as a function of the thickness for each detector, one can get the relationship of the sensitivity to thickness. Figure 23 shows these data with a best-fit power curve which provides a general expression for the sensitivity of these sensors to iron particles as follows:

$$S = (\text{Dia})\,(\text{Vel})\,(\cos\beta)^{1.5}(\text{Thck})^{-0.875} - 1.814 \tag{10}$$

$$S > 0: \quad \text{discharge signal} \tag{11}$$

$$S < 0: \quad \text{no signal} \tag{12}$$

We caution that we have studied only iron particles in the tests mentioned. The detector sensitivity is obviously a function of the density of the projectiles used, and hence the sensitivity will change with projectile density. We would discourage simple scaling of the

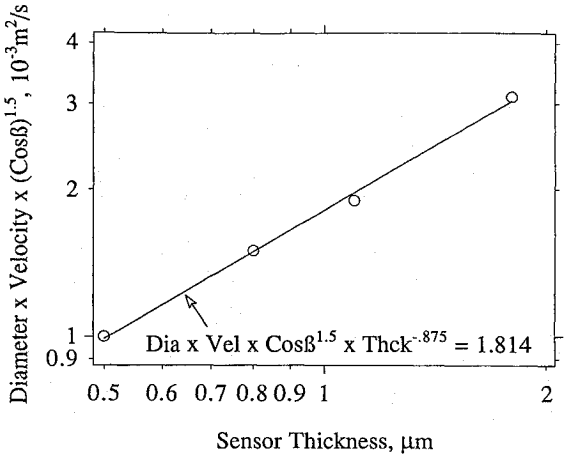

Fig. 23 Metal-oxide-silicon capacitor detectors sensitivity to iron particles.

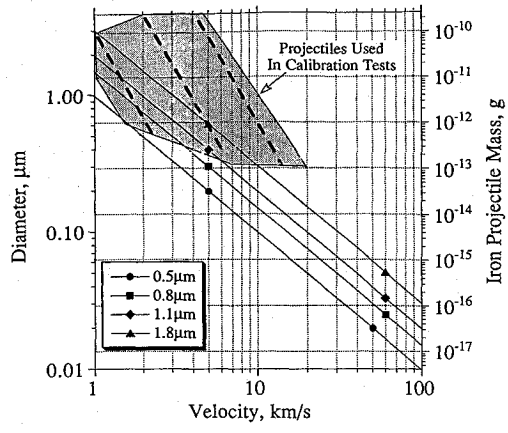

Fig. 24 Sensitivity threshold for normal impacts on various sensor thicknesses. Impacts above a line produce a signal.

mass to arrive at a new sensitivity, as that will likely be in error. Tests are needed using projectiles with different densities to determine the dependence of the sensitivity on projectile density.

Given the equation for sensitivity and the projectile parameters used in these tests (Fig. 3), one can plot the calibration for various thicknesses of detectors or angles of impact. Figure 24 is an example of such a plot for the thicknesses used in these tests and impacts at normal angle of incidence.

Discussion

Before going further it will be worthwhile to compare our results with those reported in Ref. 3. As mentioned earlier, they studied both silicon dioxide and silicon nitride as the dielectric and found that both dielectrics worked. However, the detectors with silicon nitride were found to be leaky. The authors concluded that the leakage was probably due to the quality of the silicon nitride, which should not therefore be necessarily ruled out as a dielectric material. They also did not detect any significant difference between using Al and Au for the top electrode material. Although we studied only silicon dioxide as the dielectric and Al as the top electrode, we have repeated some of the tests reported in Ref. 3, with the same general results.

As shown by the impact tests reported here and in the past, the capacitor detectors respond to an impacting projectile in two different modes: 1) such that a low-level signal is obtained and the damaged area of the capacitor is limited to the impact crater region, with little or no evaporation of the top electrode outside the impact crater, and 2) such that a large signal (a significant portion of the applied capacitor voltage) is obtained, accompanied by significant evaporation of the top electrode around the impact crater. Because of the erratic nature of the low-level signals, we have concentrated on characterizing the detectors when operated in the discharge mode where the capacitor is partially discharged and a large signal is produced. For example, there has been no attempt to correlate the magnitude of low-level signals with the mass or velocity of impacting particles. The primary questions that have been considered are 1) can the detectors be operated so that they reliably record impacting events, and 2) what is the threshold for detection as a function of particle mass, velocity, and angle of impact?

The breakdown mechanisms responsible for producing the signal are obviously very complex, with a number of factors participating at various stages of the discharge event. First, the actual discharge mechanism is not monitored, since it is an internal mechanism and only the recharge current or sensor voltage can be measured. The impact of a high-velocity projectile on a capacitor-type detector generates very high pressures and temperatures (shock waves) in the capacitor as well as in the projectile. The high pressures resulting from the shock wave cause electromechanical breakdown of the dielectric. This can occur either through the mechanical collapse of the dielectric, or if the intrinsic strength of the dielectric is exceeded. In either case there is a threshold pressure or shock that is needed to trigger the event. Temperature also causes changes in the mechanical as well as the electrical properties of the dielectric. Consequently, the nature of the projectile as well as its mass and velocity affect the shock wave (as does the temperature of the target) and hence the threshold for breakdown. In the tests reported here the effect of temperature on the threshold of detector sensitivity was not pursued.

Although pressure or shock is the initiating mechanism for the discharge, it is not adequate to explain a sustained discharge. A second mechanism must be invoked if the discharge is to be sustained for any period of time. One way to model the discharge is to consider the impacted area of the capacitor to be a resistor in parallel with the capacitor—this assumes the impact area is small compared to the total capacitor area, which is the case here. With this assumption, the discharge must be sustained for a time greater than approximately 3 times the value of the parallel resistor times the capacitance if complete discharge is to occur. This second mechanism contributing to the capacitor discharge is related to the large quantity of energy (voltage) stored in the capacitor and available to sustain cascade ionization in the shocked region of the capacitor immediately following impact. The material in the impact region will be highly ionized, so there are free electrons throughout the impact region, and hence the plasma region may act like a metallic conductor.

Experimentally, the discharges are observed to be accompanied by a flash of light, which confirms the presence of a plasma. We did not investigate specifically whether or not light could be seen in cases where a low-level signal was observed. One way of locating the position of an impact is to observe where the flash of light occurs when the apparatus is operated in the discharge mode. Rarefaction waves from the impact can also add to the luminosity of the plasma. As mentioned earlier, when a new detector is first formed, it often has electrical shorts caused by imperfections in the dielectric. These shorts are removed by applying voltage to the capacitor, which causes the shorted region to burn out. As these defects are removed, they are often accompanied by a flash of light.

There is yet another mechanism that limits the amount of discharge the capacitor experiences. This mechanism is controlled by the metal type and thickness of the top electrode as well as the applied voltage. Since the metal is thin by design, it is not capable of sustaining high current densities for any significant time, on account of resistive heating. As the capacitor discharges through the short caused by the impact, the energy dissipated by the metal electrode simply heats the metal to the point that it evaporates, leaving an open circuit to the shorted region. This is a valuable attribute of detectors of this type, since it renders the detector ready to count again if it is being used as an event counter. The area of this burnout is dependent on the applied voltage; the larger the discharge signal, the larger the burnout area. Figure 12 indicates a linear relationship (for higher bias voltages) between the amount of aluminum removed and the signal energy. From these data, one can calculate the ratio of signal energy to mass of aluminum removed (238 kJ/g) and compare this with the amount of thermal energy (13.6 kJ/g) required to vaporize aluminum at 300 K. This comparison indicates that vaporizing aluminum accounts for less than 10% of the signal energy.

In summary, we have identified three mechanisms that play a role in the discharge of these detectors: 1) initiation of the discharge by the projectile, 2) limited continuation of the discharge by the plasma created by the impact, resulting in low-level (millivolt) signals for low applied voltages, and 3) discharges sustained by the stored energy in the capacitor, which last long enough to evaporate away a portion of the top metal electrode around the impact region, thereby opening the electrical circuit to the impacted area. The energy stored in the capacitor is clearly seen to play a significant role in the discharge mechanism, since it controls the area over which the top-electrode metal is vaporized and removed. This is also seen by comparing the magnitude of the discharge energy with that of the projectile, where the maximum kinetic energy of the projectiles used in this study was approximately 6×10^{-6} J while the discharge energy was as much as 2×10^{-4} J.

From a theoretical view, it has not been possible to develop a model based on physical principles that can be used to describe the discharge mechanisms and the detector response to projectile parameters such as mass and velocity. At first glance one would think that it might be possible to relate the detector sensitivity to crater depth or diameter. If this were possible, then one could take advantage of existing work on cratering theory such as that given by Öpik[7] and Gault.[8] For example, Ref. 8 empirically scaled parameters with kinetic energy (mv^2) raised to a power between 0.370 and 1.133, depending on the parameter of interest, such as the penetration depth. In Ref. 7 parameters were scaled with a slightly lower power of the impact velocity, more closely resembling momentum (mv) rather than energy. As can be seen in our empirical formulation for sensitivity, the mass-velocity relationship is mv^3, which is a stronger function of velocity than is kinetic energy.

Conclusion

Based on the present work and that of previous researchers,[3] we have shown that it is possible to build detectors of the MOS capacitor type that can be used as event counters to measure hypervelocity particle impacts that are above a given sensitivity threshold. For use as an event counter, bias voltages large enough to cause significant discharge of the capacitors are required. Each event removes a small portion of the detector. However, the area is so small (20–60 μm in diameter) compared to the area of the detectors (2-in. diameter) that unless thousands of impacts are counted, the damage can be neglected.

Although it has not been possible to develop an analytical expression for the detector sensitivity based on a theoretical knowledge of the discharge mechanisms, it has been possible to fit an empirical expression to the data as shown in Figs. 18–23. Detectors of this type, 0.5 and 1.1 μm thick, were used on the Interplanetary Dust Experiment (IDE) that was flown on the Long Duration Exposure Facility. The calibration data presented in this paper are useful in determining the size or mass of the particles that produced the impact signals recorded by the IDE.

When the IDE was returned to earth, after $5\frac{1}{2}$ years in space, the 1.1-μm detectors still had sufficient bias to be operational. An optical survey of the impact sites on these detectors provided average-flux data for the full LDEF mission.[9] However, the battery that provided bias for the 0.5-μm detectors was completely discharged, and these detectors became inactive some time after the first year in orbit. Both the laboratory test described in this paper and the space experiments like IDE/LDEF are required to develop the instrumentation needed to monitor and study space debris and the natural micrometeoroid environment. We believe, and the MTS and LDEF missions have shown, that detectors of the type described here are very reliable and offer a means of obtaining data on the flux of meteoroid and space debris in the low mass range, where it has been very difficult to obtain real-time data in the past.

References

[1]D'Aiutolo, C. T., Kinard, W. H., and Naumann, R. J., "Recent NASA Meteoroid Penetration Results from Satellites," *Meteor Orbits and Dust*, edited by Gerald S. Hawkins, NASA SP-135, 1967, pp. 239–251.

[2]Canady, K. S., Monteith, L. K., and Donovan, R. P., "Characterization of Silicon Oxide for a Capacitance-Type Meteoroid Penetration Detector," Contract No. NAS1-7949, Research Triangle Inst., NASA CR-66712, Sept. 1968.

[3]Brooks, A. D., Parker, C. D., and Monteith, L. K., "Study of Meteoroid Detection Systems Applicable to the Outer Planets Missions," Contract No. NAS1-11692, Research Triangle Inst., NASA CR-132310, Oct. 1973.

[4]Kassel, P. C., "Characteristics of Capacitor-Type Micrometeoroid Flux Detectors When Impacted with Simulated Micrometeoroids," NASA D-7359, Nov. 1973.

[5]Singer, S. T., et al., "First Spatio-Temporal Results from the LDEF Interplanetary Dust Experiment," *Advances in Space Research*, Vol. 11, No. 12, 1991, pp. 115–122.

[6]Golub, R. A., and Davidson, J. R., "Micrometeoroid Impact Simulation System," *Space Simulation*, edited by J. C. Richmond, Special Publication 336, National Bureau of Standards, Oct. 1970, pp. 915–933.

[7]Öpik, E. J., "The Moon's Surface," *Annual Review of Astronomy and Astrophysics*, Vol. 7, 1969, pp. 473–526.

[8]Gault, D. E., "Displaced Mass, Depth, Diameter, and Effects of Oblique Trajectories for Impact Craters Formed in Dense Crystalline Rocks," *The Moon*, Vol. 6, No. 1, 1973, pp. 32–44.

[9]Simon, C. G., Mulholland, J. D., Oliver, J. P., Cooke, W. J., and Kassel, P. C., "Long-Term Microparticle Flux Variability Indicated by Comparison of Interplanetary Dust Experiment (IDE) Timed Impacts for LDEF's First Year in Orbit with Impact Data for the Entire 5.77-Year Orbital Lifetime," *LDEF—69 Months in Space: Second Post-Retrieval Symposium*, edited by Arlene S. Levine, NASA CP-3194 Part 2, April 1993, pp. 693–703.

R. K. Clark
Associate Editor